Effect of Nonlinear Thermal Radiation on MHD Stagnation Point Flow of a Carreau Nanofluid with a Homogeneous/Heterogeneous Chemical **Reaction Past a Stretching Plate** 

<sup>1</sup>Dr. V. Rohini, <sup>2</sup>Dr. P. Vidhya, <sup>3</sup>Dr. M. Petchaiammmal, <sup>4</sup>O. A. Sridevi, <sup>5</sup>Mrs. M. Maheswari, <sup>6</sup>Dr. S. R. Chitra

<sup>1</sup>Professor, <sup>2</sup>Associate Professor, <sup>3</sup>Associate Professor, <sup>4</sup>Assistant Professor, <sup>5</sup>Head and Assistant Professor, <sup>6</sup>Head and Associate Professor <sup>1,2</sup> Department of Physics, Science and Humanities, Nehru Institute of Engineering and Technology, Coimbatore, India

<sup>3</sup>Department of Chemistry, DMI College of Engineering, Chennai, India <sup>4</sup>Department of Chemistry, Karpagam Institute of Technology, Coimbatore, India <sup>5</sup>Department of Physics, Noble College of Arts and Science for Women, Palavanatham, Virudhunagar, India

<sup>6</sup>Department of Physics, P K N Arts and Science College, Thirumangalam, Madurai, India

Corresponding Author: S. R. Chitra

**Abstract:** This study analyses the Brownian effects and thermophoresis characteristics on the stagnation point flow of magnetohydrodynamic viscoelastic materials across a horizontal permeable plate with nonlinear thermal radiation. The impact of homogeneous/heterogeneous models is used to assess the analysis of heat and mass transmission processes. The ordinary differential system is used to reinterpret the physically modelled statements. The Galerkin weighted residual method (GWRM) is used to construct this restructured model quantitatively. The calculated findings are shown visually, and the comparison benchmark with previously published results provides a limited feeling of validity for the current solutions. As the values of the thermophoresis and Brownian motion parameters increased, our studies revealed the opposite tendency. Additionally, it is seen that the shear stress rate at the wall increases with rising temperature ratio parameter values and decreases with increasing ratio parameter numbers. Because of the presence of nanoparticles that increase thermal capacity, the current work is found to be beneficial in the manufacturing of glass fibre, sugar solution, and radiator engine cooling.

**Keywords:** Carreau nanofluid; Homogenous/heterogeneous chemical reaction; Nonlinear thermal radiation; Suction/injection

#### 1. Introduction

Many researchers have given the study of non-Newtonian fluid models a great deal of thought because to the practical requirements in industry and technology, including the manufacturing of glass fibre, sugar solution, mud, condensed milk, etc. The features of the theological fluid cannot be adequately described by a single mathematical model due to the variety of the non-Newtonian fluid. These mathematical models included the Maxwell model, the Casson model, the power-law model, and others. The Carreau fluid model was the non-Newtonian fluid model that was being examined. The Carreau fluid model resulted in the powerlaw's incapacity to study fluid at both extremely low and extremely high shear rates. Molecular network theories of rheological equations were initially introduced by Carreau [1].

One well-known group of researchers who worked on Carreau nanofluid was Eid et al. [2], who used numerical methods to study flow over a porous nonlinear stretching surface. The 4th-5th Runda-Kutta-fehlbery method, which is based on the shooting approach, was used to solve the equation. Their analysis suggests that the heat transfer rating decreases as the thermal radiation parameter increases, although the concentration distribution shows the reverse trend. The Carreau nanofluid of unsteady flow was investigated numerically with varying conductivity by Irfan et al. [3]. Khan et al. [4] took into consideration the model for extrusion systems time-dependent flow study of Carreau nanofluid across an accelerating surface with gyrostatic microscopic organism.

The numerical solutions are calculated using the built-in MATLAB Solver bvp4c. Hashim [5] examined the nature analysis of multiple Carreau nanofluid material flow due to shrinking geometry with heat transfer. As the temperature drops, the magnetic parameter rises to second solutions. The impact of zero mass flux of nonlinear radiation on MHD Carreaunan of fluid flow at the surface over a radially expanding surface was investigated by Lu et al. [6]. According to the study, nonlinear radiation rises with temperature distribution, whereas the concentration profile of nanoparticles decreases as chemical and heat generating values increase. Using the fourth-fifth order Range-KuttaDahlberg method with shooting method, Kumar et al. [7] demonstrated nonlinear thermal radiation with slip effects on Carreau nanofluid on a stretched magnetic flow. The study demonstrates that an increase in the Brownian motion parameter Nb results in an increase in the rates of mass and heat transfer. The partial slip and buoyancy-induced blood-gold Carreau nanofluid was examined by Olubode et al. [8]. Using the Chebyshev special collocation method, Sobamowo et al. [9] reported flow and heat transmission in an MHD dissipative Carreau nanofluid with internal heat generation across a stretching plate sheet. According to the study, the heat transfer rate was increased by raising the power-law and unsteadiness. Bibi et al. [10] talked about a hybrid nanofluid Carreau magnet that uses a lubrication technique to address homogeneous/heterogeneous

chemical reactions utilising a homotopy-based package called BVPH 2.0. According to the study, fluid velocity decreases as Weissenberg and Hartina numbers rise.

Non-Newtonian fluids undergoing chemical reactions have recently attracted the attention of scientists and engineers. There are two types of chemical reactions: homogeneous and heterogeneous. When the stimulus is in the same phase, a chemical reaction is said to be homogeneous; when the stimulus is in a different phase, a reaction is said to be heterogeneous. Heterogeneous stimuli happen in solid states, while homogenous stimuli happen in gaseous states. In combustions and biochemical systems where the catalyst surface is consumed and produced within the fluid, a very complicated reaction takes place on the catalyst surface due to the interplay between homogenous and heterogeneous chemical reaction flow. For simple isothermal flow, Chaudhary and Merkin [11] model homogeneous-heterogeneous responses under boundary layer flow. The effect of homogeneous and heterogeneous chemical reactions on the stagnation flow of an MHD micropolar with slip velocity in a permeable medium across a strengthened/shrinking surface was investigated by Reddy and Euneetha [12]. The obtained equations were numerically solved using the Matlab bvp4c packages.

For both homogeneous and heterogeneous processes, the data display distinct behaviours in terms of solute concentration at the surface. Using the Keller box method, Malik et al. [13] examined overstretching in a cylinder with a heterogeneous chemical reaction in a Williamson fluid model. In a comparison analysis, Ali et al. [14] calculated 3D cross-fluid flow and examined the impact of homogenous - heterogeneous chemical reaction models. The investigation shows that the velocity profile behaves more when the radiation and heat source are both present. One of the parameters rises. The effects of a homogeneous-heterogeneous chemical reaction on the flow of a silver-water nanofluid across a cylindrical nonlinear stretch with Newtonian heating were documented by Suleman et al. [15]. The shooting technique is used to solve the problem numerically, and for the mounting value of the magnetic parameter, the temperature distribution rises while the velocity field's decreases. Akaje and Olajuwon have investigated the effects of a heat source and an angled magnetic field on the dynamics of swimming microorganisms in blood flow saturated with nanoparticles. [16]. According to the aforementioned analysis, not much research has been done on the combined effects of nonlinear thermal radiation and homogenous-heterogeneous chemical reactions in a Carreau nanofluid. Thus, the purpose of this study is to investigate how the buoyancy effect and nonlinear thermal radiation affect the stagnation point flow of an MHD Carreau nanofluid with homogenous-heterogeneous chemical reaction.

Furthermore, no research has been done on how nonlinear thermal radiation affects the MHD stagnation point of non-Newtonian nanofluid flow with homogeneous or heterogeneous components. One of the weighted residual approaches (Galerkin method) is used to produce the numerical computational result. A graphic analysis and discussion of the mathematical model's parameters' physical meaning are presented.

#### 2. Mathematical Formulation

Examine a two-dimensional, incompressible Carreau nanofluid boundary layer stagnation point flow above a stretching permeable surface.

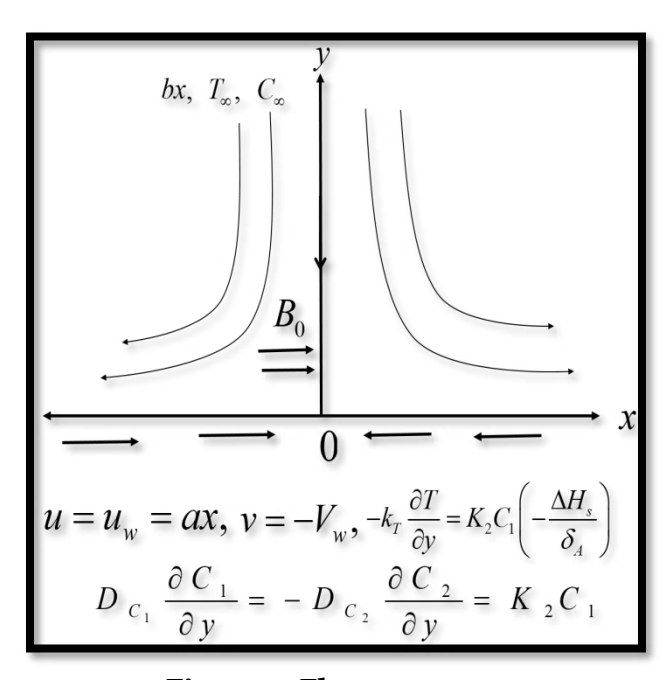


Figure 1: Flow geometry

The effects of magnetic fields and nonlinear thermal radiation are used. The isothermal cubic autocatalytic reaction is taken in the manner (Chaudhary and Merkin [11] and Merkin [17])

$$A + 2B \rightarrow 3B$$
, rate =  $k_1 C_1 C_b^2$  (1)

The first-order isothermal reaction on the surface is expressed as

$$A^* \rightarrow B^*$$
, rate =  $k_2 C_1$  (2)

The governing equations for two-dimensional flow can be put into the forms Hayat et' al. [18]:

$$\frac{\partial u}{\partial x} + \frac{\partial v}{\partial y} = 0,$$

$$u \frac{\partial u}{\partial x} + v \frac{\partial u}{\partial y} - U_{\infty} \frac{dU_{\infty}}{dx} = v \frac{\partial^{2} u}{\partial y^{2}} \left[ 1 + \Lambda^{2} \left( \frac{\partial u}{\partial y} \right)^{2} \right]^{\frac{n-1}{2}} + v (n-1) \Lambda^{2} \left( \frac{\partial u}{\partial y} \right)^{2} \frac{\partial^{2} u}{\partial y^{2}} \left[ 1 + \Lambda^{2} \left( \frac{\partial u}{\partial y} \right)^{2} \right]^{\frac{n-3}{2}} + v \left( \frac{\partial u}{\partial y} \right)^{2} \frac{\partial^{2} u}{\partial y^{2}} \left[ 1 + \Lambda^{2} \left( \frac{\partial u}{\partial y} \right)^{2} \right]^{\frac{n-3}{2}} + v \left( \frac{\partial u}{\partial y} \right)^{2} \frac{\partial^{2} u}{\partial y^{2}} \left[ 1 + \Lambda^{2} \left( \frac{\partial u}{\partial y} \right)^{2} \right]^{\frac{n-3}{2}} + v \left( \frac{\partial u}{\partial y} \right)^{2} \frac{\partial^{2} u}{\partial y^{2}} \left[ 1 + \Lambda^{2} \left( \frac{\partial u}{\partial y} \right)^{2} \right]^{\frac{n-3}{2}} + v \left( \frac{\partial u}{\partial y} \right)^{2} \frac{\partial^{2} u}{\partial y^{2}} \left[ 1 + \Lambda^{2} \left( \frac{\partial u}{\partial y} \right)^{2} \right]^{\frac{n-3}{2}} + v \left( \frac{\partial u}{\partial y} \right)^{2} \frac{\partial^{2} u}{\partial y^{2}} \left[ 1 + \Lambda^{2} \left( \frac{\partial u}{\partial y} \right)^{2} \right]^{\frac{n-3}{2}} + v \left( \frac{\partial u}{\partial y} \right)^{2} \frac{\partial^{2} u}{\partial y^{2}} \left[ 1 + \Lambda^{2} \left( \frac{\partial u}{\partial y} \right)^{2} \right]^{\frac{n-3}{2}} + v \left( \frac{\partial u}{\partial y} \right)^{2} \frac{\partial^{2} u}{\partial y^{2}} \left[ 1 + \Lambda^{2} \left( \frac{\partial u}{\partial y} \right)^{2} \right]^{\frac{n-3}{2}} + v \left( \frac{\partial u}{\partial y} \right)^{2} \frac{\partial^{2} u}{\partial y^{2}} \left[ 1 + \Lambda^{2} \left( \frac{\partial u}{\partial y} \right)^{2} \right]^{\frac{n-3}{2}} + v \left( \frac{\partial u}{\partial y} \right)^{2} \frac{\partial^{2} u}{\partial y^{2}} \left[ 1 + \Lambda^{2} \left( \frac{\partial u}{\partial y} \right)^{2} \right]^{\frac{n-3}{2}} + v \left( \frac{\partial u}{\partial y} \right)^{\frac{n-3}{2}} \frac{\partial^{2} u}{\partial y^{2}} \left[ 1 + \Lambda^{2} \left( \frac{\partial u}{\partial y} \right)^{2} \right]^{\frac{n-3}{2}} + v \left( \frac{\partial u}{\partial y} \right)^{\frac{n-3}{2}} \frac{\partial^{2} u}{\partial y^{2}} \left[ 1 + \Lambda^{2} \left( \frac{\partial u}{\partial y} \right)^{2} \right]^{\frac{n-3}{2}} \frac{\partial^{2} u}{\partial y^{2}} \left[ \frac{\partial u}{\partial y} \right]^{\frac{n-3}{2}} \frac{\partial^{2} u}{\partial y} \left[ \frac{\partial u}{\partial y} \right]^{\frac{n-3}{2}} \frac{\partial u}{\partial y} \left[ \frac{\partial u}{\partial y} \right]^{\frac{n-3}{2}} \frac{\partial u}{\partial y}$$

$$\rho c_{p} \left( u \frac{\partial T}{\partial x} + v \frac{\partial T}{\partial y} \right) = k \frac{\partial^{2} T}{\partial y^{2}} - \frac{\partial q_{r}}{\partial y} + \left( \frac{-\Delta H_{h}}{\delta_{A}} \right) \left( k_{1} C_{1} C_{2}^{2} \right) + \tau \left( D_{B} \frac{\partial T}{\partial y} \frac{\partial C}{\partial y} + \frac{D_{T}}{T_{\infty}} \left( \frac{\partial T}{\partial y} \right)^{2} \right), \tag{5}$$

$$u\frac{\partial C_1}{\partial x} + v\frac{\partial C_1}{\partial y} = D_{C_1} \left( \frac{\partial^2 C_1}{\partial x^2} + \frac{\partial^2 C_1}{\partial y^2} \right) - KC_1 C_2^2 + \frac{D_T}{T_{\infty}} \frac{\partial^2 T}{\partial y^2}, \tag{6}$$

$$u\frac{\partial C_2}{\partial x} + v\frac{\partial C_2}{\partial y} = D_{C_2} \left( \frac{\partial^2 C_2}{\partial x^2} + \frac{\partial^2 C_2}{\partial y^2} \right) + KC_1 C_2^2 + \frac{D_T}{T_\infty} \frac{\partial^2 T}{\partial y^2}, \tag{7}$$

with the boundary conditions

$$u = u_w = ax, v = -V_w, -k_T \frac{\partial T}{\partial y} = K_2 C_1 \left( -\frac{\Delta H_s}{\delta_A} \right), D_{C_1} \frac{\partial C_1}{\partial y} = -D_{C_2} \frac{\partial C_2}{\partial y} = K_2 C_1 \quad \text{at } y = 0$$
 (8)

$$u = u_{\infty} \to bx, \ v = 0, \ T \to T_{\infty}, \ C_1 \to C_{\infty}, \ C_2 \to 0 \quad \text{as} \ y \to \infty$$
 (9)

Magyari and Pantokratoras [24] defined the radiative heat flux as

$$q_r = -\frac{4}{3} \frac{\sigma}{\overline{k}} \frac{\partial T^4}{\partial y} = -\frac{16}{3} \frac{\sigma}{\overline{k}} \frac{\partial}{\partial y} \left( T^3 \frac{\partial T}{\partial y} \right) \tag{10}$$

where  $\sigma$  and  $\overline{k}$  are the Stefan-Boltzmann constant and the mean absorption coefficientrespectively, and with Eq. (5), the heat balance equation becomes

$$\rho c_{p} \left( u \frac{\partial T}{\partial x} + v \frac{\partial T}{\partial y} \right) = k \frac{\partial^{2} T}{\partial y^{2}} + \frac{16}{3} \frac{\sigma}{\overline{k}} \frac{\partial}{\partial y} \left( T^{3} \frac{\partial T}{\partial y} \right) + \left( \frac{-\Delta H_{h}}{\delta_{A}} \right) \left( k_{1} C_{1} C_{2}^{2} \right) + \tau \left( D_{B} \frac{\partial T}{\partial y} \frac{\partial C}{\partial y} + \frac{D_{T}}{T_{\infty}} \left( \frac{\partial T}{\partial y} \right)^{2} \right), \quad (11)$$

With the help of the similarity variable in agreement with Akinbo and Olajuwon [19]

$$u = axf'(\eta), \ v = -\sqrt{av}f(\eta), \ \eta = \sqrt{\frac{a}{v}}y, \ g(\eta) = \frac{C_1}{C_\infty}, \ h(\eta) = \frac{C_2}{C_\infty},$$

$$\theta(\eta) = \frac{T - T_\infty}{\Delta T}, \Delta T = T_w - T_\infty, \ \Delta C = C_w - C_\infty$$
(12)

Eq. (1) is satisfied identically, the model is reduced to

$$\left[1 + nWe(f'')^{2}\right]\left[1 + We(f'')^{2}\right]^{\frac{n-3}{2}}f''' + ff'' - (f')^{2} + M^{2}(A - f') + A^{2}$$
(13)

$$\left(\left(1+Rd\left(1+\left(\theta_{w}-1\right)\theta\right)^{3}\right)\theta'\right)'+\Pr\left(f\theta'+\Pr\left(N_{b}\theta'\phi'+N_{t}\theta'^{2}\right)+\gamma gh^{2}=0\right)$$
(14)

$$g'' + Scfg' - k_s gh^2 + \frac{N_t}{N_b} \theta'' = 0,$$
(15)

$$\delta h'' + Scfh' + k_s gh^2 + \frac{N_t}{N_b} \theta'' = 0,$$
(16)

and the transformed boundary conditions:

$$f'(0) = 1, \ f(0) = f_w, \quad \theta'(0) = -K_T g(0), \ g'(0) = K_s g(0), \quad -h'(0) = \frac{K_s}{\delta} g(0),$$
 (17)

$$f'(\infty) = A, \quad \theta'(\infty) = 0, \quad g(\infty) = 1, \quad h(\infty) = 0, \quad \phi(\infty) = 0.$$
 (18)

where

$$f_{w} = \frac{V_{w}}{\sqrt{av}}, \operatorname{Pr} = \frac{v}{\alpha}, \operatorname{Rd} = \frac{16\sigma T_{\infty}^{3}}{3\overline{k}k} Sc = \frac{v}{D_{A}}, K = \frac{k_{1}C_{\infty}^{2}}{a}, A = \frac{b}{a}, \delta = \frac{D_{B}}{D_{A}}, \gamma = k_{1} \left(\frac{\Delta H_{h}C_{\infty}^{3}}{\rho C_{p}\delta_{A}a\Delta T}\right), We = \frac{\Lambda^{2}a^{3}x^{x}}{\alpha}, K_{s} = \frac{k_{s}}{D_{A}} \sqrt{\frac{a}{v}}, M^{2} = \frac{\sigma B_{0}^{2}}{\rho a}, Nt = \frac{\tau D_{T}\left(T_{w} - T_{\infty}\right)}{vT_{\infty}}, Nb = \frac{\tau D_{B}\left(C_{w} - C_{\infty}\right)}{v}, K_{T} = \frac{k_{s}C_{\infty}}{K_{T}\Delta T} \left(\frac{\Delta H_{s}}{\delta_{A}}\right) \sqrt{\frac{a}{v}}, K_{T} = \frac{k_{s}C_{\infty}}{k_{T}\Delta T} \left(\frac{\Delta H_{s}}{\delta_{A}}\right) \sqrt{\frac{a}{v}}$$

Suction/injection, Prandtl number, Radiation parameter, Schmidt number, homogenous strength of reaction, ratio parameter, diffusion coefficient, homogenous and heterogeneous buoyancy ratio, Weissenberg number, the heat homogenous reaction, non-Newtonian parameter, buoyancy ratio, the heterogeneous strength of the response, magnetic field framework, thermophoresis framework, Brownian motion, and thermal conductivity with regard to homogenous reaction are the names of the parameters defined in Eq : Let assume that the diffusion type coefficients  $D_{C_1}$  and  $D_{C_2}$  are equivalent

i.e.  $\delta = 1$  and this gives

$$g(\eta) + h(\eta) = 1, \tag{20}$$

Concerning that, the model with the help of the above Eq. (20) is given as

$$\left[1 + nWe(f'')^{2}\right]\left[1 + We(f'')^{2}\right]^{\frac{n-3}{2}}f''' + ff'' - (f')^{2} + M^{2}(A - f') + A^{2}$$
(21)

$$\left(\left(1 + \frac{4Rd}{3}\left(1 + \left(\theta_w - 1\right)\theta\right)^3\right)\theta'\right)' + \Pr f\theta' + \Pr \left(N_b\theta'\phi' + N_t\theta'^2\right) + \gamma g\left(1 - g\right)^2 = 0$$
(22)

$$\frac{1}{Sc}g'' + fg' - kg(1-g)^2 + \frac{N_t}{N_b}\theta'' = 0,$$
(23)

$$f'(0) = 1, f(0) = f_w, \quad \theta'(0) = -K_T g(0), \quad g'(0) = K_s g(0),$$
 (24)

$$f'(\infty) = A, \quad \theta'(\infty) = 0, \quad g(\infty) = 1.$$
 (25)

For the case of practical concern, the dimensionless physical quantities are the coefficient of skin friction and the Nusselt number and are expressed as

$$C_{fx} = \frac{\tau_w}{\rho U_w^2}, \ Nu_x = -\frac{xq_w}{k(T_w - T_{co})}.$$
 (26)

where

$$C_{fx} = \frac{\tau_w}{\rho U_w^2} \bigg|_{y=0}, \quad Nu_x = -\frac{x}{\left(T_w - T_\infty\right)} \left(\frac{\partial T}{\partial y}\right)_{y=0} + q_r. \tag{27}$$

$$q_{w} = k \left(\frac{\partial T}{\partial y}\right)_{y=0} + \left(q_{r}\right)_{w}; \ \tau_{w} = \eta \frac{\partial u}{\partial y} \left[1 + \Lambda^{2} \left(\frac{\partial u}{\partial y}\right)^{2}\right]^{\frac{n-1}{2}} \bigg|_{y=0}.$$

$$(28)$$

With the help of Eq. (12) and after simplification, the dimensionless form is reduced to

$$\operatorname{Re}_{x}^{\frac{1}{2}}C_{fx} = f''(0)\left[1 + We^{2}\left(f''(0)\right)^{2}\right]^{\frac{n-1}{2}}; \operatorname{Re}_{x}^{-\frac{1}{2}}Nu_{x} = -\left(1 + Rd\theta_{w}^{3}\right)\theta'(0); \tag{29}$$

### 3. Method of Solution

An engineering tool for estimating solutions to boundary value issues is the weighted residual method, which is highly effective in resolving both linear and coupled nonlinear differential equations.

The Galerkin weighted residual method (GWRM) is one of the weighted residual techniques that Finlayson and Scriven [20] studied and investigated. The weighted residual approach is used by Odejide and Aregbesola [21] to address semi-infinite domain problems. Oderinu and Aregbesola [22], Aregbesola [23], and Ghesemi et al. [24] are more contributors to the approaches.

## The basic steps in Galerkin weighted residual methods(GWRM) are:

(i) Obtained an appropriate solution to the differential equation of the form:

$$L(u(y)) + f(y) = 0$$
 on  $\partial \Omega$  (30)

Where u(y) stands for the unknown dependent variable, f(y) stands for the independent function of the domain  $\partial\Omega$  and L stands for the differential operator.

(ii) The function  $\varphi$  (i.e. solution) is presumed to satisfy both the operator equation and the boundary conditions.

A trial function of the form

$$\varphi = \varphi_0 + \sum_{k=1}^n a_i \varphi_k \tag{31}$$

where  $a_i$  constants are to be determined. We select a trial function in a way that satisfies the boundary conditions including those at infinity. We include a function such as  $e^{-nx}$  for n > 0 in the trail function which will make the trail function naturally satisfy the boundary condition.

Substituting equation (31) into equation (30) resorts to residual function R(y). (iii) The main focus of weighted residual R(y) is to minimize the value in the domain  $\partial\Omega$  by integrating the product of the weighted function  $\varphi_k$  and residual function R(y) over the domain  $\partial\Omega$ .

$$\int_{\Omega} \varphi_k R(x) dx = 0, \quad k = 0, 1, \dots n$$
(32)

- We then applied the Gauss- Laguerre formula to get a system of algebraic (iv) equations by integrating each of the equations in equation (32). The Gauss-Laguerre is used because of its usefulness in the boundary condition ranges of zero to infinity.
- (v) solutions are then sorted by solving the equations utilizing MATHEMATICA a computer-assisted symbolic package.

## 3.1 Formula for Gauss - Laguerre.

The formula Gauss - Laguerretakes the form

$$\int_{0}^{\infty} e^{-y} f(y) dy \approx \sum_{j=1}^{n} B_{j} f(y_{j})$$
(33)

The argument  $y_i$  being the zeros of the  $n^{th}$  Laguerre polynomial

$$L_n(y) = e^y \frac{d^n}{dy^n} \left( e^{-y^n} \right) \tag{34}$$

and the coefficient  $B_i$  being

$$B_{j} = \frac{\left(n!\right)^{2}}{y_{j} \left[L_{n}\left(y_{j}\right)\right]^{2}} \tag{35}$$

We now obtain the values of constants  $a_i, b_k$  and  $c_k$  by solving the algebraic equations usinga mathematical package named MATHEMATICA a computer-assisted symbolic package.

Table 1: Comparison of values of A when n=1; M=0

Α	Pop et al. [25]	Sharma and Singh	Hayat et al.	Present
		[26]	[27]	
0.1	-0.9694	-0.96939	-0.96939	-0.969386
0.2	-0.9181	-0.91811	-0.91811	-0.918107
0.5	-0.6673	-0.66726	-0.66726	-0.667263
0.7		-0.43346	-0.43346	-0.433477
0.8		-0.29929	-0.29929	-0.299390
0.9		-0.15458	-0.15458	-0154717
1.0		0.00000	0.00000	0.000000

### 4. Result Discussion

GWRM has been used to investigate the impact of nonlinear thermal radiation on the stagnation point flow of MHD Carreau nanofluid with homogeneous/heterogeneous chemical reactions with suction/injection boundary conditions. Diffusion coefficient, homogenous and heterogeneous buoyancy ratio, heat homogenous reaction, non-Newtonian parameter, buoyancy ratio, heterogeneous strength of reaction, magnetic field parameter, thermophoresis parameter (N<sub>t</sub>), Brownian motion parameter (N<sub>b</sub>), Suction/injection, Schmidt number (S<sub>c</sub>), Prandtl number (P<sub>r</sub>), Radiation parameter (R<sub>d</sub>), homogenous strength of reaction (K), ratio parameter (A), and thermal conductivity are among the parameters that are graphically revealed in relation to : A graphic representation of each parameter's impact on the skin friction coefficient and Nusselt numbers is provided.

## 4.1 Dimensionless velocity fields $f'(\eta)$

The impact of ratio parameter A, suction/injection parameter S, and Weissenberg number parameter We on the velocity profileare shown in Figures 2–4 respectively. A rise in the values of the ratio parameter (A) brings an upsurge to the dimensional velocity as shown in figure 2 which augments the thickness of the momentum boundary layer. The velocity boundary layers thickenand exhibit different behaviours for A> 1 and A < 1. For A < 1 the stagnation velocity of the sheet is less than the stretching velocity.

For A = 1, some velocity movement was noticed for the fluid and sheet hence no boundary layer formation is feasible. Figure 3 depicts the impact of suction  $(f_w)$ , A Large value  $f_w$  is found to diminish the boundary layer's thickness because of the heavy flow of the fluid. The impact of the Weissenberg number (We) decelerates in velocity profiles as shown in Figure 4as (We) increases. The physics behind this is that the increment in the values of the (We) viscoelasticity effect is magnified within the boundary layer which consequently lowers the motion of the fluid. This observation is similar to that of Irfan et al [3].

# 4.2 Dimensionless temperature fields $\theta(\eta)$

Figures (5) - (14) illustrate the influence of ratio parameter (A), suction/injection parameter  $(f_w)$ , the heat homogenous reaction (Ks), thermal conductivity concerning homogenous reaction (Kt), Brownian motion parameter (Nb), thermophoresis parameter (Nt), Prandtl number (Pr) Radiation parameter (Rd), The ratio of ambient fluid temperature to a temperature at the wall  $(Q_w)$  and The homogeneous strength parameter (K). We observed that an increase in the parameters causes a decline in the ratio parameter (A), suction/injection parameter  $(f_w)$ , the heat homogenous reaction (Ks), Brownian motion parameter (Nb), Prandtl number, (Pr) and The homogeneous strength parameter (K) while thermal conductivity concerning homogenous reaction (Kt),

thermophoresis parameter (Nt), Radiation parameter, (Rd) and The ratio of ambient fluid temperature to a temperature at wall  $(Q_w)$  leads to increment on the temperature field  $\theta(\eta)$  which agreed with Lu et al[6]. Figure 5 reported the behaviour of the ratio parameter (A) on the dimensionless temperature. It is observed to decline the dimensionless temperature which consequently deteriorates thermal layer thickness. Figure 6.The presence of the Suction parameter ( $f_w > 0$ ) depicts the effect of suction ( $f_w$ ) on dimensionless temperature. The large value of suction  $(f_w)$  moves the motion of the fluiddecline with a rise in the ratio parameter. Figures. 7 and 8display the behaviours of the heterogeneous strength of reaction parameter (Ks) and the thermal conductivity for homogeneous reaction (Kt) on temperature fields  $\theta(\eta)$ . Opposite behaviour was noticed between both parameters on the temperature field. The thermal layer thickness decreases for the heterogeneous strength parameter when the homogeneous reaction parameter (Kt) is increased.

The opposite behaviour was also noticed for both the Brownian motion parameter (N<sub>b</sub>) and thermophoresis parameter (Nt) in Figures 9 and 10 as the values (Nb) increase the temperature field graph decreases while that of Brownian motion (Nb) increases. Figure 11 presents the effect of the Prandtl number (Pr) on temperature profiles. This figure reveals that an increase in the Prandtl number (Pr) results in a decrease in the temperature distribution. The Prandtl number defines the ratio of momentum diffusivity to thermal diffusivity hence it shows the dominance of thermal diffusivity on the temperature profiles on the Prandtl number (Pr) which is in line with Akinbo and Olajuwon[18].

The impact of the radiation parameter is shown in Figure 12. The thickness of the thermal boundary layer is shown to rise with an increase in the radiation parameter. Figure 13 illustrates the impact of the ambient temperature to wall temperature ratio in the temperature region. As long as the system's other variables stay constant, the high value intensifies the temperature gradient. The behaviour of the response parameter K's homogenous strength on temperature profiles is shown in Figure 14. According to Malik et al. [13], increasing the homogenous strength of the reaction parameter K from 0.1 to 0.5 results in a physical decrease in the thickness of the thermal boundary layer.

## 4.3 Dimensionless concentration fields $g(\eta)$

The effects on the concentration profile of parameters A, Ks, Kt, S, Nb, Nt, and Sc are explained. As the ratio parameter in the flow grows, Figure 15 illustrates how the concentration barrier layer thickens. The effects of Ks, Kt, K, and S on the concentration profiles are shown in Figures (16) through (19). As Ks and K increase, the concentrations in the boundary layer decrease, and as Kt and S increase from 0.1 to 0.5, the concentration boundary layer thickens. The behaviours of thermophoresis parameters and Brownian motion were depicted in Figures (20)-21). While a higher value of the thermophoresis

parameter thickens the concentration boundary layer, a higher value of the Brownian motion parameter decreases it. These two elements exhibit completely different behaviours on the concentration profile. The impact of Schmidt number (Sc) on the concentration profile is depicted in Figure (22). The concentration layer experiences a thickening of the border layer when the Schmidt number rises.

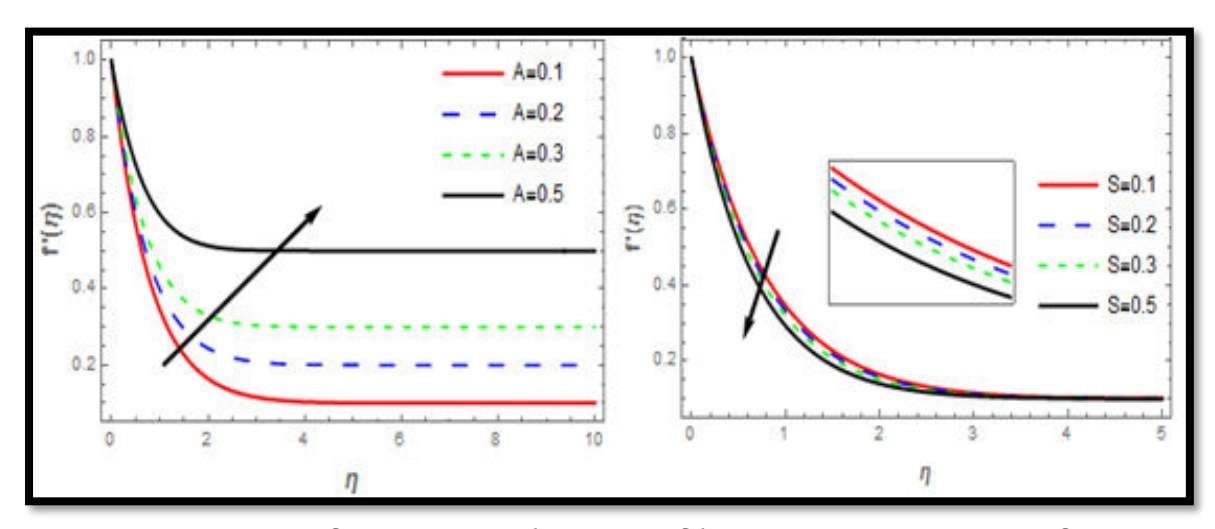


Figure 2: Variation of A against Velocity Profile; Figure 3: Variation of S against **Velocity Profile** 

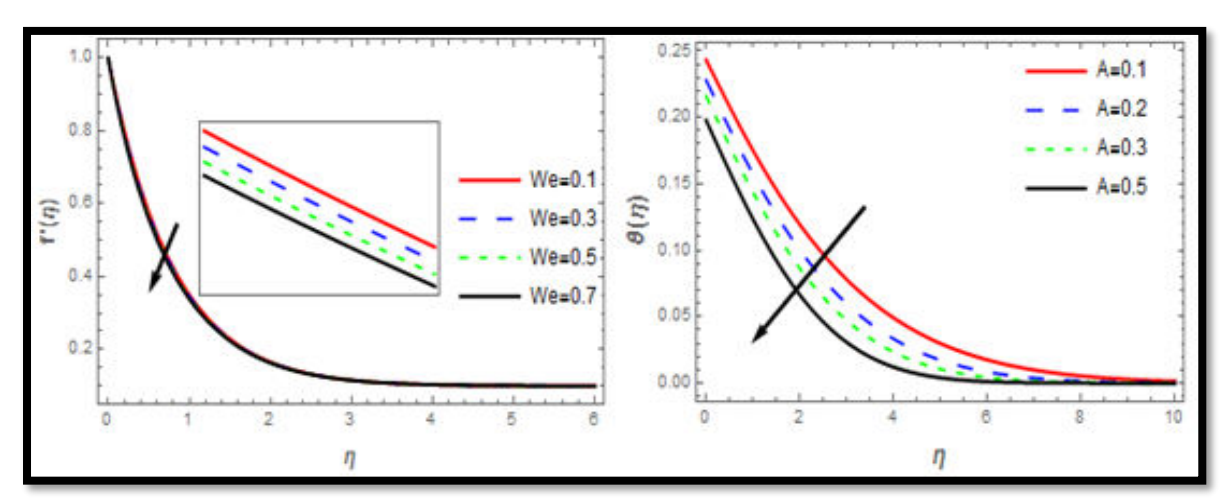


Figure 4: Variation of We against Velocity Profile; Figure 5: Variation of A against **Temperature Profile** 

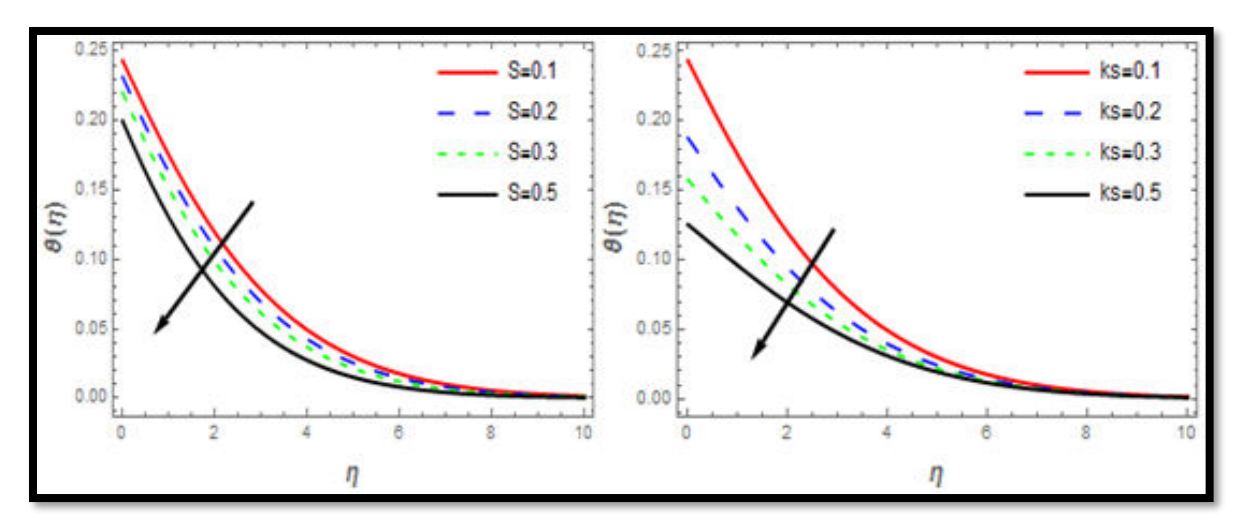


Figure 6: Variation of S against Velocity Profile; Figure 7: Variation of Ks against **Temperature Profile** 

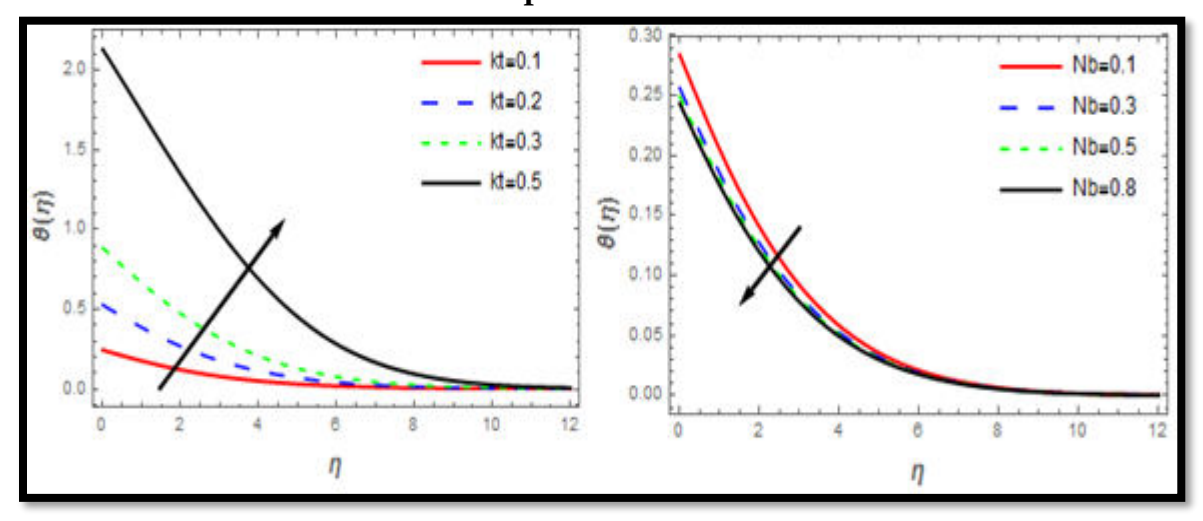


Figure 8: Variation of Kt against Temperature Profile; Figure 9: Variation of Nb against Temperature Profile

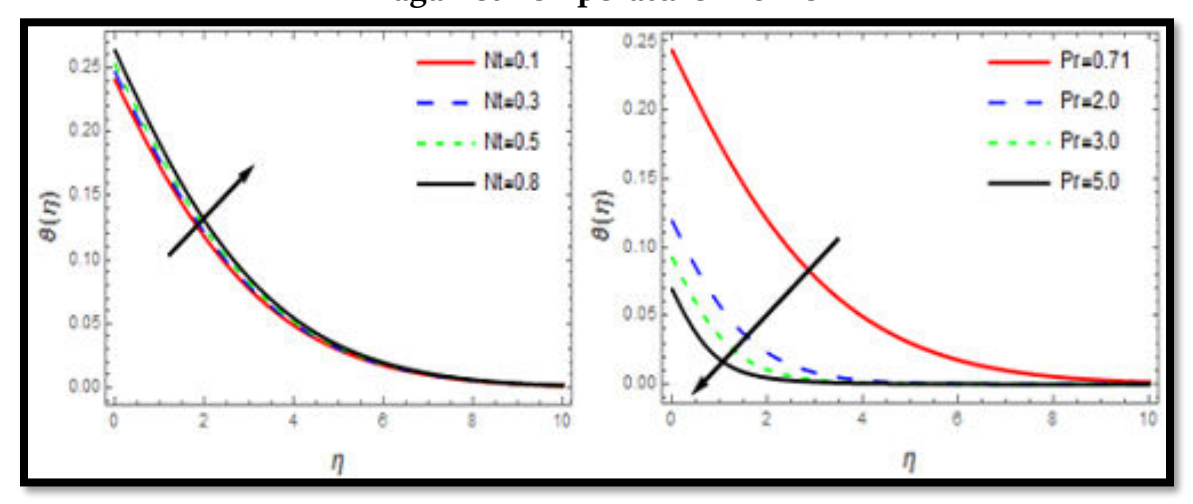


Figure 10: Variation of Nt against Temperature Profile; Figure 11: Variation of Pr against Temperature Profile

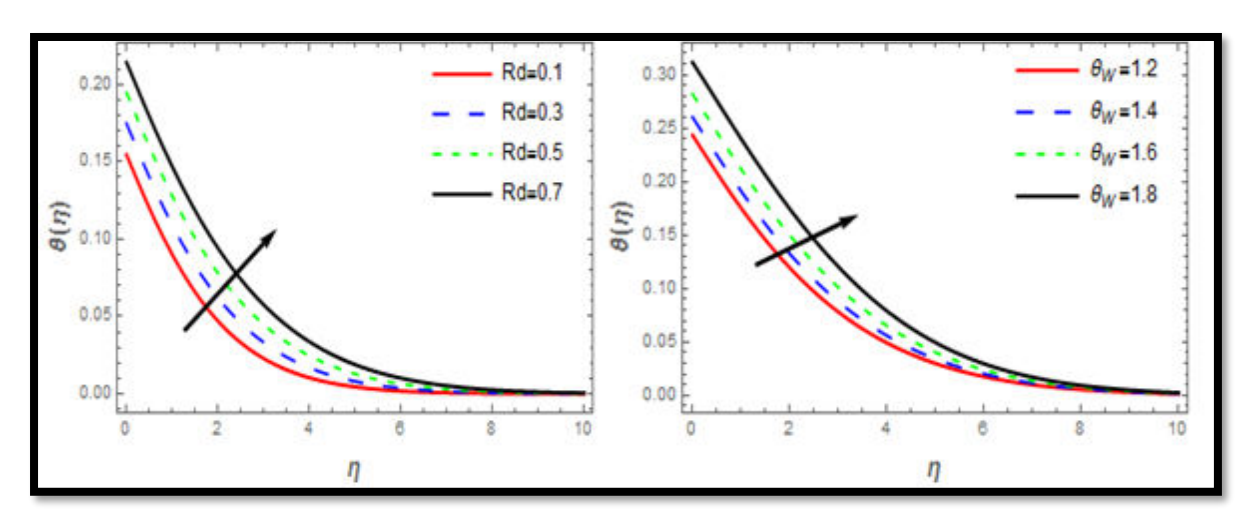


Figure 12: Variation of Rd against Temperature Profile; Figure 13: Variation of θw against Temperature Profile

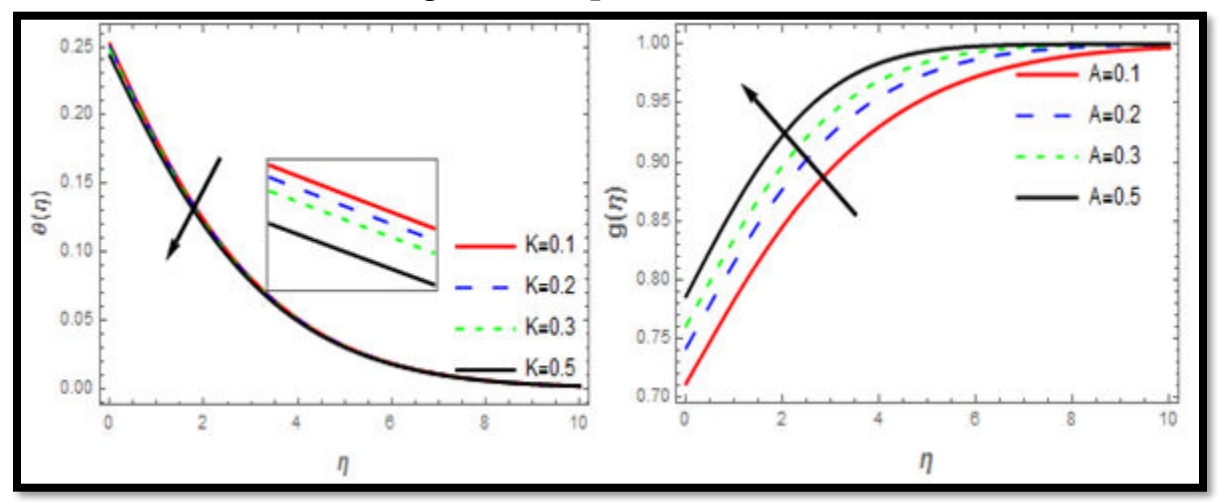


Figure 14: Variation of K against Temperature Profile; Figure 15: Variation of A against Concentration Profile

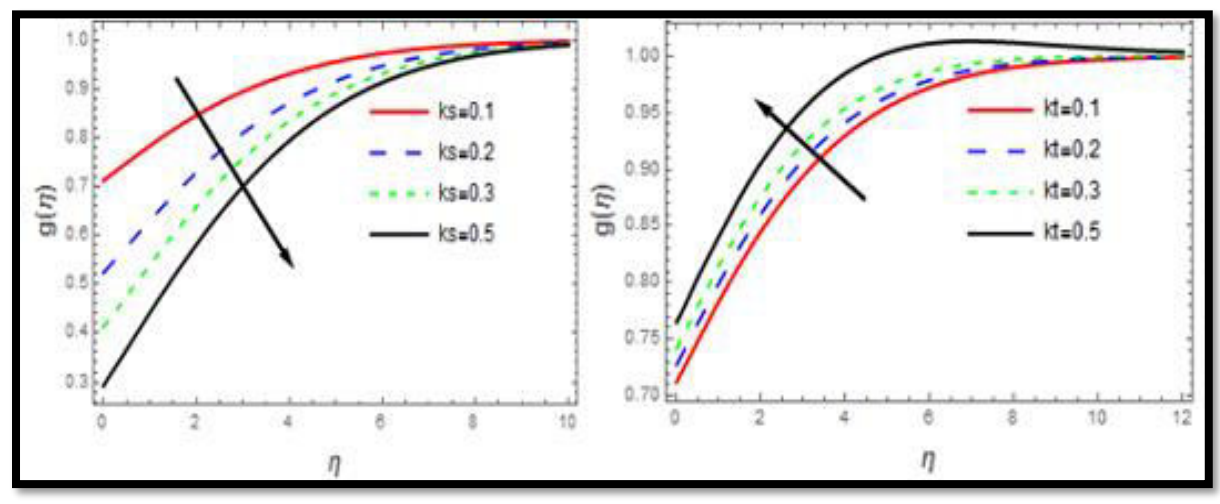


Figure 16: Variation of Ks against Concentration Profile; Figure 17: Variation of Kt against Concentration Profile

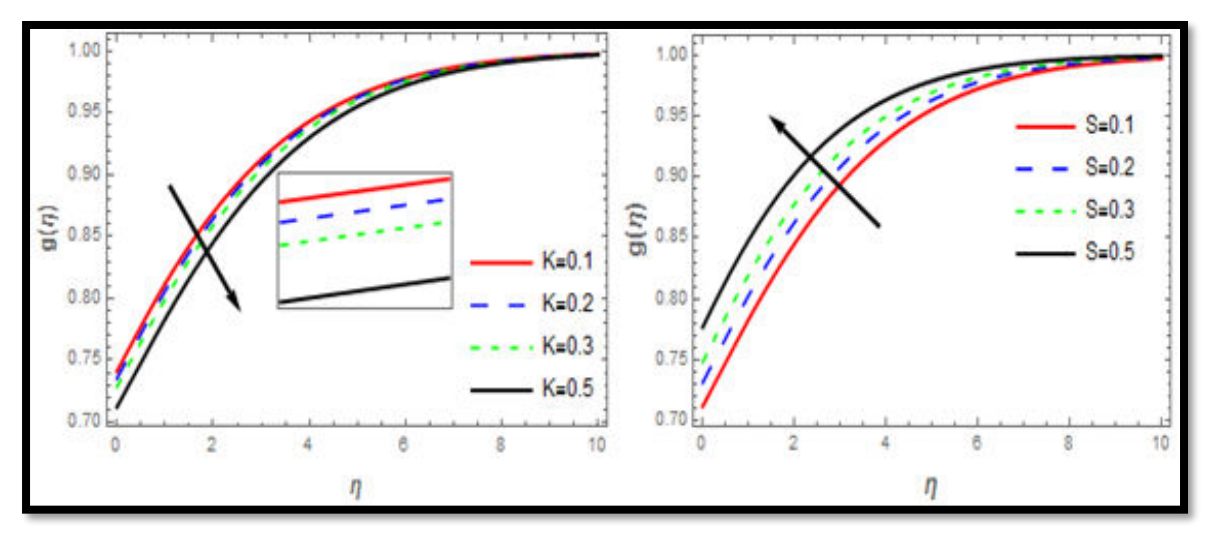


Figure 18: Variation of K against Concentration Profile; Figure 19: Variation of S against Concentration Profile

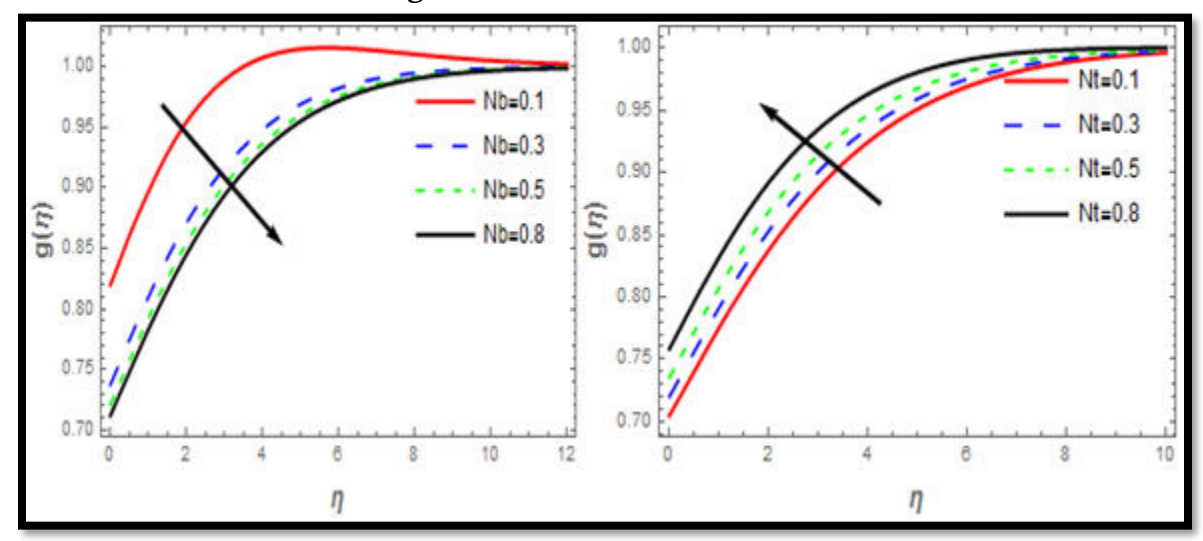


Figure 20: Variation of N against Concentration Profile; Figure 21: Variation of Nt against Concentration Profile

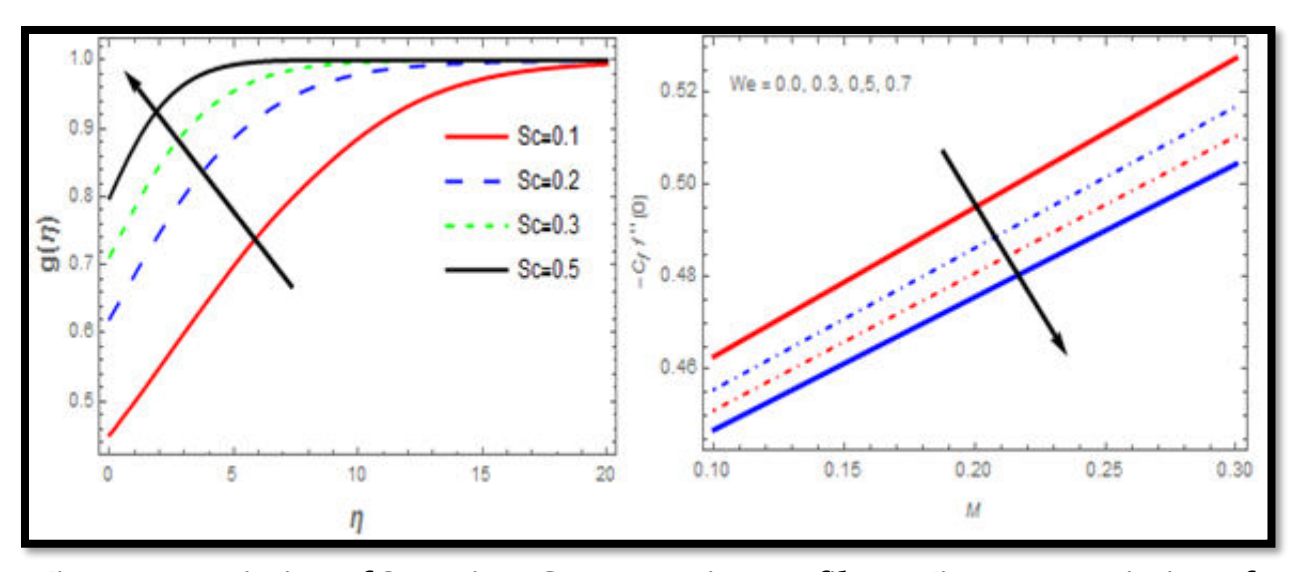


Figure 22: Variation of Sc against Concentration profile M; Figure 23: Variation of Skin friction with file for different values of We

## 4.4 Dimensionless skin friction $C_f$ and Nusselt number

Figures (23) through (24) show how controlling parameters affect skin friction. The effects of non-Newtonian parameters and the magnetic field on skin friction are displayed in Figure (23).

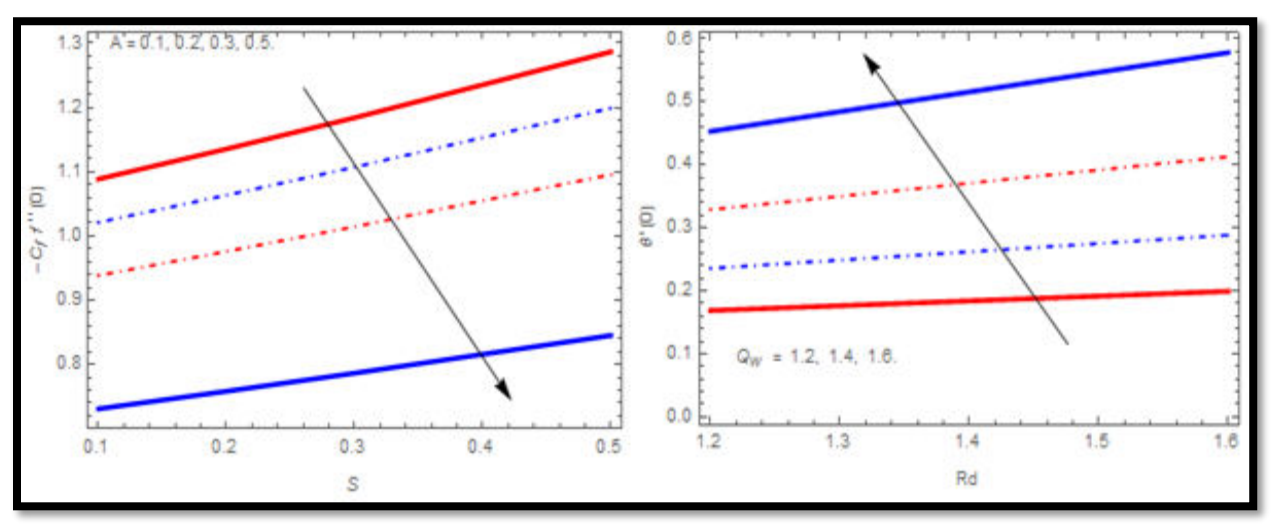


Figure 24: Variation of Skin friction with S for different values of A; Figure 25: Variation of Nusselt number with Rd for different values of  $\theta_w$ 

Shear stress and momentum transfer increase as a result of the skin friction that is intensified by the magnetic field. An increase in velocity gradient is thought to be the cause of the skin friction coefficient's rise due to a non-Newtonian parameter. Figure (24) shows that as suction parameters increase, skin friction increases as well. Skin friction increases as a result of increased momentum transfer and shear stress brought on by an

increase in these parameters. In the meantime, skin friction is reduced by parameter strengthening. An increase in the velocity gradient is the cause of this trend. Figure (25), which shows the effect of the parameter and on the Nusselt number.

#### Conclusion

Using the weighted residual approach (Galerkin method), the effect of nonlinear thermal radiation on the MHD stagnation point flow of a Carraeunanofluid across a stretching plate with homogenous/heterogeneous chemical reaction is investigated. A list of the main findings is provided below:

- The velocity field decreases with an upsurge in Weissenberg number (We)
- The heterogeneous strength of the reaction parameter(Ks) and the thermal conductivity for homogeneous reaction(Kt) shows opposite behaviourin both temperature and concentration profiles.
- A rise in the radiation parameter causes the thickness of the thermal boundary layer to increase.
- The thermal boundary layer thickness diminishes when the homogeneous strength of the reaction parameter *K* is increased.
- The concentration in the boundary layer shrinks with a rise in the values of the heterogeneous strength of the reaction parameter (Ks) and the homogeneous strength of the reaction parameter *K* is increased.
- A rise in the Brownian motion parameter diminishes the concentration boundary layer and a rise in the value of the thermophoresis parameter thickens the concentration boundary layer.
- The skin friction coefficient is enhanced withthe upsurge in magnetic field and suction parameter while the skin friction coefficient diminishes with the enhancement of parameter A.
- Nonlinear radiation and the ratio of ambient temperature towards wall temperature results enhanced the local Nusselt number.
- The shear stress rate at the wall is noticed to upsurge for greater values of temperature ratio parameters and decline for an increasing number of ratio parameters.

#### Reference

- 1. Carreau PJ. Rheological Equations for molecular network theories. Trans. sec Rhol. 1972;116:99 - 127.
- 2. Eid, MR, Mshny KL, Taseer M, Sheicholeslami M.Numerical Treatment for Carreau nanofluid flow over a porous nonlinear stretching surface. Results in physics.2018; 8:1185 - 93.

- 3. Irfan M, Raafiq K, Khan, M. Numerical analysis of unsteady Carreaunanofluid floor with variable conductivity. Springer 2020.
- 4. Khan SU, Shehzad SA. Analysis for the time-dependent flow of Carreau nanofluid over an accelerating surface with gyrotactic micro-organisms model for extrusion systems. Advances in mechanical engineering. 2019.
- 5. Hashim Multiple nature analysis of Carreau nanomaterial flow due to shrinking geometry with heat transfer. Appl. Nanosci.2020;10:3303-14.
- 6. Lu D, Ramzan M, UlHndsN, Chring. JD. (2018). Nonlinear radiation effect on MHD Carreaunanofluid flows over a radically stretching surface with zero mass flux at the surface. Sci Rep. 2018; 8:3709.
- 7. Kumar KGR, Giressh, BJ,Rashad AM.(2019).On Stretched Magnetic floor of Carreau nanofluid with slip effects and nonlinear thermal radiation. Nonlinear Engineering. 2019;8: 340 - 49 issues.
- 8. Olubode KK, Animasaun, I.L, MahantheshB.(2018) Heat transfer in the flow of blood-gold Carreau nanofluid induced by partial ship and buoyancy. Heat transfer - Asian Research. 2018;47: issue 6.
- 9. Sobamowo MG, Jayesimi LO, Waheed, MA. (2019). Chebyshev Special collocation method for flow and heat transfer in magnetohydrodynamic dissipative Carreau nanofluid over on stretching sheet with internal Heat generation. AUT. J. of Mech. Engineering. 2019;3:3-14.
- 10. Bibi A, Hang, Xu,(2018). Peristaltic Channel flow and heat transfer of Carreau magnetic hybrid nanofluid in the presence of homogenous/heterogeneous reaction.
- 11. Chandhaby M.A, Markin, JH (1995). Simple isothermal model for homogeneous heterogeneous reactions in boundary-layer flow. 1 equal diffusivity fluid dynamics reactions in research.1995;16:311-33.
- 12. Reddy. PBA, Euneetha, S. Effects of the homogenous-heterogeneous chemical reaction and slip velocity on MHD stagnation flow of a micropolar fluid over a permeable stretching/shrinking surface embedded in a porous medium. Frontiers in Heat and Mass Transfer. 2017; 8:24 - 35.
- 13. Malik MY, Salahuddin T, Arif, H. (2019). Homogenous -Heterogeneous reactions in the Williamson fluid model over a stretching cylinder by using the Keller box method.
- 14. Ali, M., Sultan, F., Shahzad, M. (2020). Influence of homogenous-heterogeneous reactions model for 3D cross fluid flow. A comparative study. Indian J Phys.2019.
- 15. Suleman M., Ramzan M, Ahmad S, Lu D.(2019). Numerical simulation for homogenous-heterogeneous reactions and Newtonian heating in silver-water nanofluid flow past a nonlinear stretched cylinder Phys sir.2020; 94. 085702.

- 16. Akaje T.W., Olajuwon B.I (2023). Dynamics of a swimming microorganism onnanoparticle-saturated blood flow under the influence of inclined magnetic field and heat source. Volume 15, Issue 3, 2023, pp. 1-22,
- 17. Merkin, J. H (1996). A model for isothermal homogeneous heterogeneous reactions in boundary layer flow, Math.Comput. Model. 1996;24:125 - 136.
- 18. Hayat T, Khan MI, Imtiaz M. AlseadA. (2017). Impacts of constructive and destructive chemical reactions in magnetohydrodynamic (MHD) flow of Jeffrey liquid due to nonlinear radially stretched surface. J.Mol.225. 2017;302 -10
- 19. AkinboBJ,Olajuwon BI.(2020). Homotopy investigation of heat and mass transfer flow past a vertical porous medium in the presence of a heat source. Int. J. Heat and Technology. 37(3):899-908
- 20. Finlayson BA., Scriven LE (1966) The method of weighted residual method A review. ApplMech Rev.1966; 19(9):735-48.
- 21. Odejide S, Aregbesola YAS. Application of Method of Weighted Residuals to Problems with Semi-Infinite Domain.Rom. Journ.Phys., 2011;14-24.Nos. 1 – 2.
- 22. Oderinu RA, Aregbesola YAS. The weighted residual method in a semi-infinite domain using un-partitioned methods. Int J Appl Math. 2012; 25(1):25-31.
- 23. Aregbesola, Y.A.S.(2003) Numerical Solution of Bratu Problems using Weighted Residuals, Electronic Journal of Southern African Mathematical Sciences Association (SAMSA). 2003;3:1 – 7.
- 24. Ghesemi PM, Abbasi M. Khaki M. New Analytic Solution of MHD fluid flow of fourth-grade fluid through the channel with slip condition via collocation method. Int J Adv Math Mech. 2015; 2(3):87-94.
- 25. Pop SR., Grosan T, Pop, I.(2004) Radiation effects on the flow near stagnation point of a stretching sheet.
- 26. Sharma PR., Sinh G. Effects of variable thërmal conductivity and heat source/sink on MHD flow near a stagnation point on a linearly stretching sheet. Appl, Fluid Mech.2009; 2:13-21.
- 27. Hayat T,Khan MI, Imtiaz M,Alsaed A. Heat and mass transfer analysis in the stagnation region of Maxwell fluiid with chemical reaction over a stretched surface. Thermal science appl. 2017; 1 – 19.